Observation of S-wave scattering of fermions accross a Feshbach resonance

D Genkina[1], LM Aycock[1,2], BK Stuhl[1], Hsin-I Lu[1] and IB Spielman [1]‡

[1]Joint Quantum Institute, National Institute of Standards and Technology, and University of Maryland, Gaithersburg, MD, 20899 USA
[2]Physics Department, Cornell University, Ithaca, NY 14850 USA

E-mail: spielman@umd.edu

Abstract. We present results on mapping out an s-wave Feshbach resonance in fermionic ^{40}K by directly observing atom scattering over a range of magnetic field strenghts. To optimize signal to noise, we develop techniques to interpret absorption imaging in the regime where recoil induced detuning corrections are significant. We apply these techniques to our s-wave scattering data to extract an estimate for the resonant magnetic field value. These techniques can be applied to observation of effective p-wave scattering in the presence of spin-orbit coupling in a spin polarized Fermi gas.

Keywords: Quantum gases, Atomic physics, Something else

‡ Corresponding author

1. Introduction

Feshbach resonances are a staple tool in the study of cold Fermi gases. Interatomic interactions in Bose-Einstein condensates are easily detected due to the high density of the cloud. However, the density of Fermi clouds is reduced by a factor of 10^3 from that of BECs. This makes it necessary to enhance the scattering cross section to observe any effects of interaction. Feshbach resonances allow one to tune the scattering length by changing the magnetic field. Not ony do they enable detection of interactions, but they make it possible to tune interactions from attractive to repulsive, allowing for the phase transition from the BCS to BEC regime at sufficiently low temperatures.

However, to take advantage of Feshbach resonances as a tool it is first necessary to have a good undestanding of the relationship between the bias magnetic field and the scattering cross section near a Feshbach resonance for specific species and hyperfine states. The exact value of the resonance is difficult to calculate analytically and must be determined experimentally. Currently, Feshbach resonances are mapped out by observing loss due to three-body inelastic scattering or by re-thermalization or anisotropic expansion measurements that infer the elastic scattering cross section from collective behavior of the cloud [3–5].

We collide two clouds of ^{40}K atoms in a mixture of $|9/2, -9/2\rangle$ and $|9/2, -7/2\rangle$ hyperfine states and directly image the resulting s-wave scattering halo as a function magnetic field strength. This allows us to directly observe the enhancement in scattering without relying on collective behavior. We calculate the fraction of atoms that scattered during the collision, and from this scattering fraction deduce the resonant magnetic field and width of the resonance.

The techniques developed in this experiment for observing Fermion scattering can be extended to engineering higher order partial wave interactions, as has been done for bosons [7].

However, even with Feshbach resonance enhancement of the scattering cross section, Fermi gases are dilute enough that very few atoms will scatter as a fraction of total atom number. This makes direct detection of s-wave scattering halo difficult due to detection uncertainty, which dispraportionally effects low atom numbers. In order to optimize the signal to noise for low atom numbers, we increased our imaging time. However, above saturation absorption imaging at sufficiently long exposure times poses a particular problem - if the atoms have had time to absorb enough photons such that the recoil velocity Doppler shifts them from resonance on the order of the linewidth of the resonance, this recoil-induced detuning is a significant correction to the observed absorption of the probe light. In order to take this correction into account, we simulate the imaging process and use the results to extract the atom number and the scattered fraction from our images.

This paper is in two parts. In the first, we study absorption imaging in the presence of significant recoil-induced detuning and show how we use our results to interpret data. In the second, we describe our s-wave scattering experiment and, after correcting our

data for recoil-induced detuning, extract a measure of the location of the Feshbach resonance in ^{40}K.

2. Absorption imaging in the presence of strong recoil induced detuning

Absorption imagaing is one of the two most common imaging techniques used in ultracold atomic physics, fluorescence imaging being the other. To obtain an absorption image, one shines an on or near resonant probe beam onto the atomic cloud, and captures the part of the beam that made it through the cloud onto a camera. Then, the atoms are allowed to leave the trap, and the probe light is shined directly at the camera, to calibrate the intensity of light that the atoms saw. The intensity in the second camera image at some point in time is called the initial intensity, $I_0(t)$, as it is assumed to be the intensity before interaction with atoms. The intensity in the first image at some point in time is called the final intensity, $I_f(t)$.

It is convenient to define the optical density, $\nu = -\ln \frac{\int I_f(x,y,t)\mathrm{d}t}{\int I_0(x,y,t)\mathrm{d}t}$. Assuming the intensity seen by the camera during the first and second pulse is constant in time, this reduces to $\nu = -\ln \frac{I_f(x,y)}{I_0(x,y)}$. This is an observed quantity, and it is then the job of the experimentalist to relate it to the number of atoms $n = \int \rho\,(x,y,z)\ \mathrm{d}z$, where ρ is the 3d atomic distribution, and z is the imaging axis. Another useful quantity is the optical depth, $OD = \sigma_0 \rho$, where σ_0 is the on-resonant scattering cross section. Though in general one needs a theoretical model to relate the optical density ν to the optical depth and thus the atom number, it is convenient that in the limit of zero probe intensity, these quantities coincide, $OD_0 = \nu$, as will be seen below. We call this OD_0, becaue it is the simplest, in a sense "0th order" model for relating the optical density to the optical depth.

The intensity of light from the beam as a function of distance is equal to the power scattered by the atoms. Without taking the atomic recoil velocity into account, and thus assuming both the intensity at every point in the cloud to be constant in time, this is given by [6]

$$\frac{dI(z)}{dz} = -\rho\sigma_0 \frac{I(z)}{1 + I(z)/I_{sat}}, \tag{1}$$

where I_{sat} is the saturation intensity. We've suppressed the x and y dependence, or alternatively we've focused on a single pixel. This equation can be easily integrated over z to obtain

$$OD_1 = \sigma_0 n = \nu + \frac{I_0 - I_f}{I_{sat}}, \tag{2}$$

This gives us a model for the optical depth that includes a correction due to saturation intensity. In the limit of far below saturation probe intensity, it reduces to our "0th order" model, OD_0.

Once you include the recoil velocity, the atoms become doppler shifted out of resonance and thus change the amount of proble light that will get absorbed. This

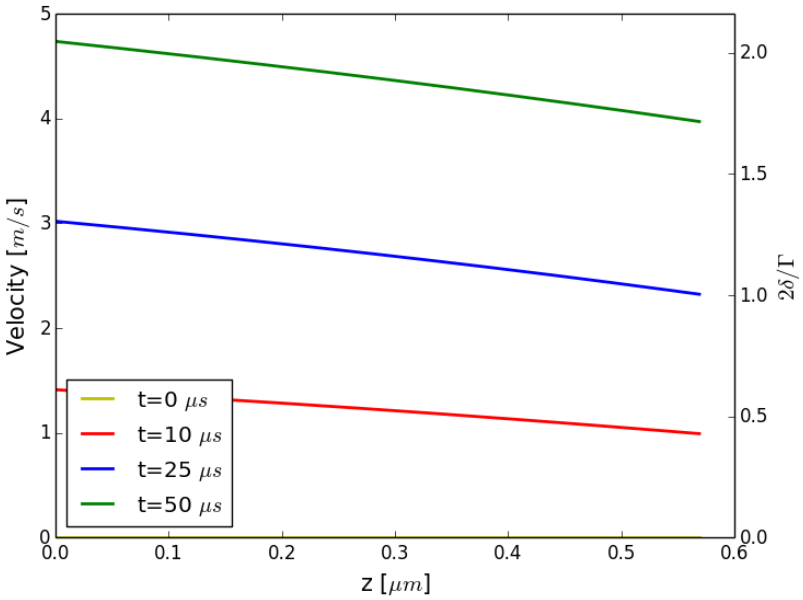

Figure 1. Distribution of generalized detuning $\Delta = \frac{2\delta}{\Gamma}$ accross an atomic cloud of ^{40}K for three different imaging times, as obtained by numerical simulation.

detuning varies both with imaging time t and distance along the propagation direction z (Figure 1). Thus, the intensity lost to the atoms also acquires a time dependence:

$$\frac{dI(t,z)}{dz} = \sigma_0 \rho \frac{I(t,z)}{1 + \frac{4}{\Gamma^2}\delta(t,z)^2 + I(t,z)/I_{sat}}, \tag{3}$$

where Γ is the linewidth of the atomic transition, and δ is the detuning, given by

$$\delta(t,z) = \frac{v_r}{\hbar c \rho} \int_0^t \frac{dI(z,\tau)}{dz} \, \mathrm{d}\tau, \tag{4}$$

where v_r is the recoil velocity. In this case, one can no longer obtain a straightforward relation between the atom number and the intensities in the two absorption images.

One can consider this equation perturbatively in time and obtain corrections to second order in imaging time, OD_2 [2]. However, the perturbative treatment breaks down after about a recoil of imaging time (Figure 2). In order to adequately correct for the recoil induced detuning of the atoms, we must simulate the process and obtain numerical predictions for I_f given a certain imaging time, atomic density, and probe intensity.

In the following, we describe two versions of this simulation. First, we take the simplistic approach that the on-axis distibution of atoms does not change dramatically durning the imaging time and can be treated statically. We test this approach in known limits and then use then check the validity of the static assumption. It turns out that, for realistic input parameters, this assumption is grossly incorrect. So, we take a slightly more sophisticated approach and allow the atoms to move within the cloud during the imaging time. This allows us to simulate the phase space evolution of atoms subjected

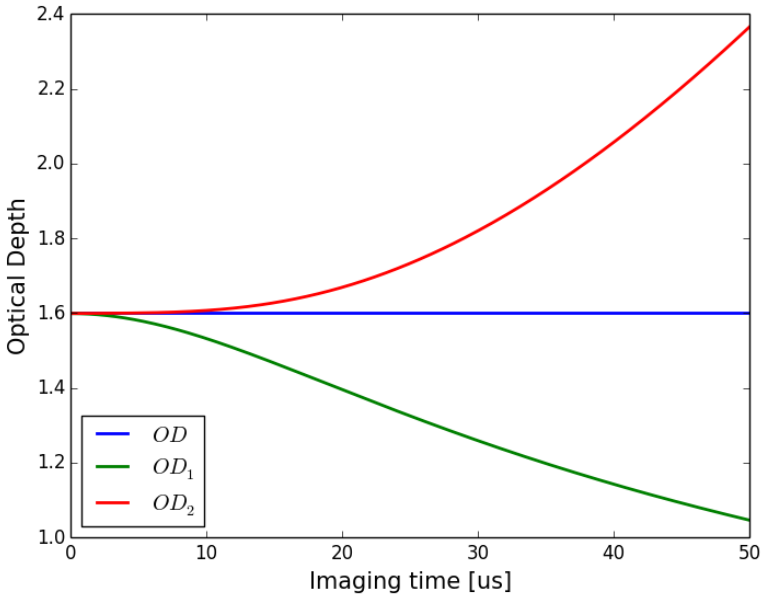

Figure 2. Using time dependent I_f values obtained from recoil detuning corrected simulation of on-resonant imaging of ^{40}K atoms, this graph shows the optical depths each model would deduce from such images. The true optical depth is given at 1.6.OD_1 is the high probe intensity corrected optical depth given by 2. OD_2 is the model that includes high probe intensity corrections and imaging time corrections from expanding 3,4 to second order in imaging time [2]. Note that the value obtained using the second order expansion in time starts to differ significantly from the true value after about 15us. The probe intensity is $0.8\, I_{sat}$.

to probe light. However, in the end we find that numerical differences in predicted OD only vary on the 0.05% level between the two models.

2.1. Stationary atom model

In order to solve eq 3,4, we start with an input 1-d distribution of atom densities $\rho(z)$, usually gaussian in shape. We divide the cloud into spatial bins (the bin size was chosen such that decreasing the bin size further produced less than a 0.001% difference in the result). Each bin carries a certain number of atoms. In this approximation, we keep the number of atoms in each bin constant. Then, we input a probe intensity, and propagate the intensity bin by bin according to 3, such that each bin only sees the probe intensity that was not absorbed in the previous bins. Then, we update the average velocity of the atoms in each bin according to 4 for our time step size dt. Then, we propagate the probe intensity through each bin again, starting with the same intensity at the first bin but this time taking into account the average recoil induced detuning of each bin in calculating the intensity aborbed. We continue this two-step process until we reach the desired imaging time.

We sum the intensity that made it through the entire cloud at each time step

$\int_{t=0}^{t_f} I_f(\tau)\,\mathrm{d}\tau$, the observable that is actually detected on the first absorption image. From this we can obtain a simulated optical density, $\nu_s = -\ln\frac{\int I_f(\tau)\,\mathrm{d}\tau}{I_0 t_f}$. This optical density depends on the initial probe intensity and the intput atom number, or optical depth. Thus, we can take our two absorption images, which give us a value for the optical density as well as I_0, and infer what optical depth would have to be put into the simulation to obtain the observed optical density. We call this inferred optical depth OD_{corr}, the optical depth corrected for recoil induced detuning effects.

To check the validity of our simulation, we can take it to certain limits in which the probelm becomes analytically solvabale. In the limit that the probe intensity is much weaker than saturation, $I_0 \ll I_{sat}$, the atoms will not absorb enough light to significantly detune from resonance. We can then neglect time dependence and 3 reduces to

$$\frac{dI(z)}{dz} = -\rho\sigma_0 I(z), \tag{5}$$

from which we recover the simple

$$\sigma_0 n = OD_0 = \nu. \tag{6}$$

In the limit that the probe intensity is much stronger than saturation, $I_0 \gg I_s at$, even far detuned atoms will absorb light at their maximum, allowing us to again neglect the time dependence and reduce 3 to

$$\frac{dI(z)}{dz} = -\rho\sigma_0 I_{sat}, \tag{7}$$

which integrates out to

$$\sigma_0 n = \frac{I_0 - I_f}{I_{sat}}. \tag{8}$$

We recognize 6 and 8 as the two terms in the expression for OD_1, 2. Thus, in both limits OD_{corr} should coincide with OD_1. Or equivalently, if the optical depth is an input parameter, in those limits both 2 and our simulation should produce the same prediction for optical density. Indeed, they coincide as seen in figure 3.

Encouraged by the reasonable behavior of our simulation, we can now use it to see if the stationary atom assumption is self consistent, ie if the distance travelled by the atoms in one bin during the imaging time is less than the bin size. However, as can be seen from figure 7, it turns out that not only do the atoms travel more than the bin size, but they also travel more than the size of the whole cloud, and the back of the cloud travels less than the beginning for long enough imaging times. Thus, the atomic distribution as a function of position changes dramatically during the imaging time, and our stationary assumption is completely invalid.

2.2. Traveling atom model

To account for the changing atomic distribution during the imaging pulse, we shift our framework slightly from spatial bins of equal size with varying atoms number to superatoms. That is, we divide the initial atomic distribution into clumps of a set

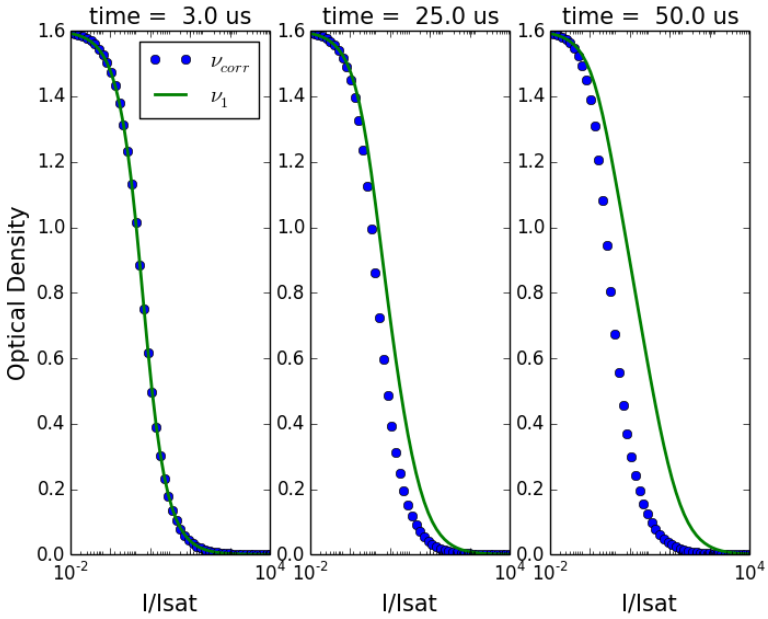

Figure 3. Optical densities as a function of probe intensity as predicted by the simulation and by 2, for three different imaging times. The predictions agree in both the high and low intensity limits, and differ for probe intensitites comparable to the saturation intensity. The difference is enhanced with increased imaging time.

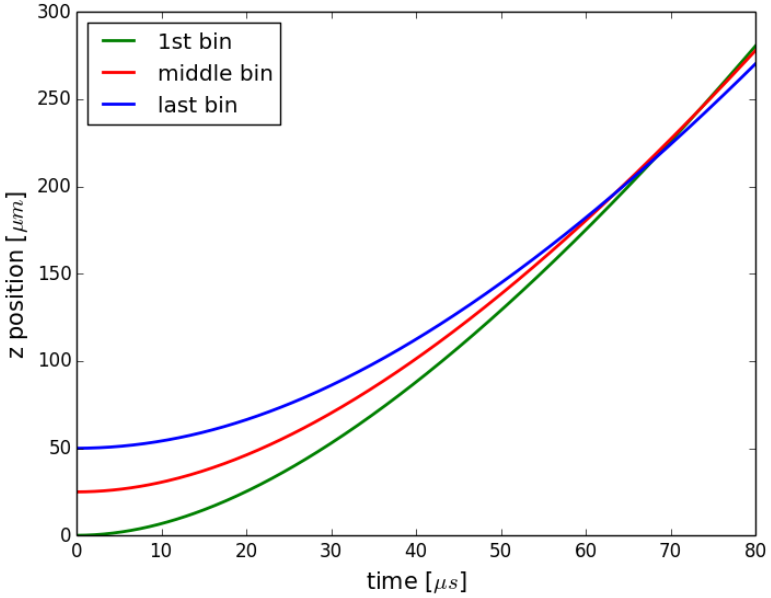

Figure 4. Position of atoms as a function of imaging time for atoms in the first, middle, and last bins of the simulation. The probe intensity here is $1.2I_{sat}$, and the optical depth is 1.6.

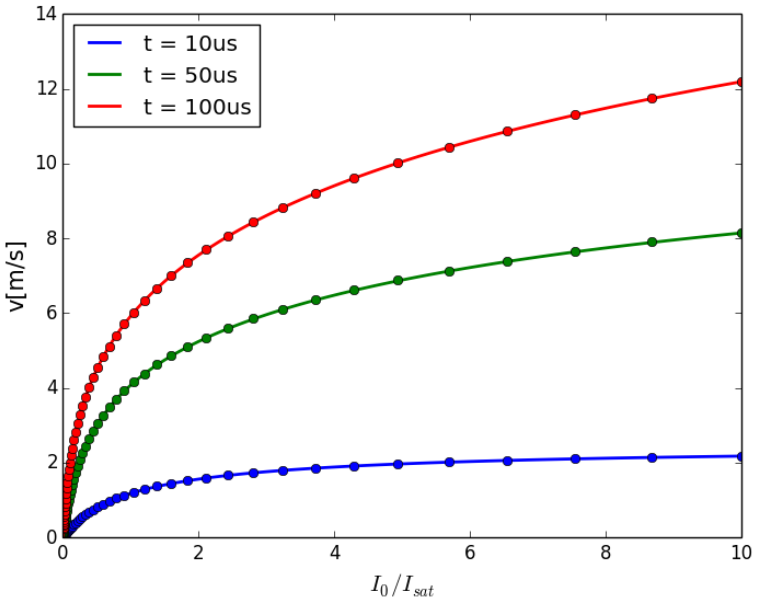

Figure 5. The velocity of a single superatom as a function of probe intensity for various imaging times. The dots represent simulation data, while the lines represent analytical solutions.

number of atoms, called superatoms, with initial positions that reflect the atomic distribution. The simulation then proceeds as before, propagating the probe light through one superatom at a time. But now, after the probe has been propagated through and the velocities of the superatoms are updated, the positions of the superatoms are advanced accordingly before the next time step is taken. Thus, we can simulate an evolving atomic distribution and track the resultant detunings.

First, we should check the velocity behavior of our superatoms against calculable limits. One such limit is that of a single supeatom. In this case, the intensity seen by the superatom is constant at the full probe intensity, and the only time dependance in the problem is in the velocity, and thus detuning, of the superatom. 4 can then be re-written as

$$\frac{d\delta\left(t\right)}{dt} = \frac{v_r}{\hbar c\rho}\frac{dI}{dz}\left(t\right) = \frac{v_r\sigma_0}{\hbar c}\frac{I_0}{1+\frac{4}{\Gamma^2}\delta(t)^2 + I_0/I_{sat}}, \tag{9}$$

or in dimensionless form,

$$\frac{d\Delta(t)}{dt} = kv_r\frac{\tilde{I}}{1+\Delta^2+\tilde{I}}, \tag{10}$$

where $\Delta = 2\delta/\Gamma$, $\tilde{I} = I_0/I_{sat}$ and k is the photonic wavevector. 10 can be integrated and solved exactly with one real root. We can compare that result to our simulation, and it agrees as seen in figure 5.

We are now in a position to study the time dependance of the cloud evolution. This can be visualized as a phase space evolution of superatoms, as seen in figure 6. We see that the cloud shape is actually strongly distorted in the imaging time.

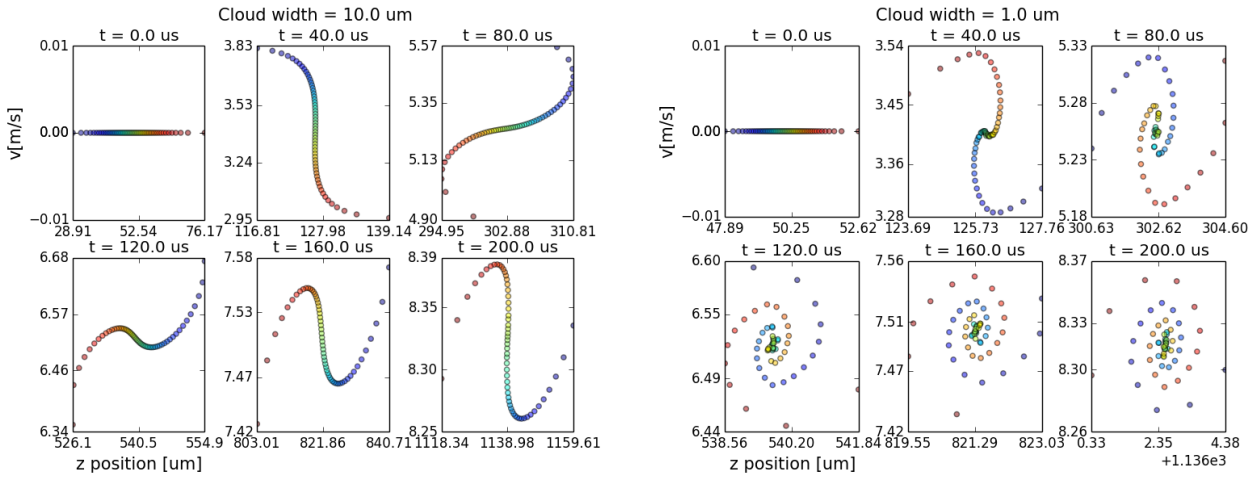

(a) (b)

Figure 6. Phase space evolution of an atomic cloud exposed to probe light of $1.2I_{sat}$. The optical depth is 1.6, and the initial cloud is a gaussian with width a. $10\mu m$ and b. $1\mu m$

Having performed both the stationary and traveling atom simulations, we can compare the optical densities predicted by each, which we call ν_{corr1} and ν_{corr2} respectively. We find that, depite the significant changes in atomic distribution during the imaging time, the predicted optical densities are so slightly changed by including this effect that it is practically undetectable. In fact, the difference $|\nu_{corr1} - \nu_{corr2}|/\nu_{corr1} \leq 0.05$. Thus, for the purposes of deducing the optical density from experimental optical depths, simply using a stationary model is sufficient. Furthermore, the actual atomic distribution $\rho(z)$ is largely irrelevant, and the only observable is the total atom number $n = \int \rho(z)\mathrm{d}z$.

2.3. Calibration of saturation intensity

Now we come to the question of how to interpret the actual ouput of an imaging camera. Each camera pixel outputs an integer number of "counts", proportional to the total energy it absobed during a pulse. The precise proportionality constant of these counts to the intensity as seen by the atoms depends on many factors, such as the quantum efficiency of the camera, the photoelectric conversion factor of the camera, and the polarization of the probe light.

The most accurate way to determine this factor is through a direct experiment. In the limit where the system is adequately described by 6, only the ratio of the initial and final intensities matters, and thus this proportionality constant is irrelevant. In all other regimes, however, the ratio of the initial and final intensities to the saturation intensity also comes into play, making the proportionality constant significant. One way to approach this is to calibrate the saturation intensity in terms of camera counts per unit time.

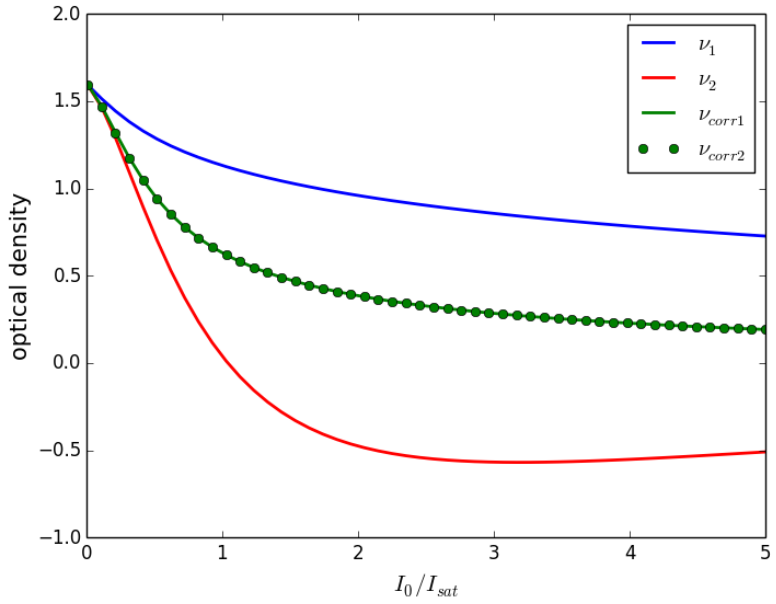

Figure 7. Predictions for optical density as a function of probe intensity for an imaging time $t = 50\mu s$. Note that the two versions of simulated optical density, ν_{corr1} and ν_{corr2} are virtually indistinguishable.

In order to calibrate the saturation intensity in camera counts per unit time, we take absorption images of a cloud of ^{40}K atoms at three different imaging times, 40us, 100us, and 200us, and at varying probe intensities. We pick a small square in the center of the cloud, where the atomic density is approximately uniform, and average the initial and final intensities of each pixel in the square. Thus, for each image we obtain one I_0 and one I_f, in units of counts per microsecond, or equavalently one optical density and one I_0/I_{sat}. We then do a least squares fit of ν_{corr}, our simulated optical density, to the data. The two fit parameters are the optical depth at the center of the cloud, representing the actual atom number, and the value of I_{sat} in counts per microsecond. As seen in figure 8, the model produces a good fit to the experimental data.

2.4. Signal to noise optimization

Now that we have the ability to interpret absorption images at larger imaging times, we can choose an imaging time based on optimal signal to noise ratio. Here, we consider only the photon shot noise that results in camera count noise, with the uncertainty proportional to $\sqrt{N_p}$, where N_p is the photon number. We then propagate this uncertainty through our correction scheme to deduce the final uncertainty in the calculated optical depth.

As seen in figure 9, around $40\mu s$ for reasonable parameters the uncertainty levels out and there are no longer appreciable benefits by extending the imaging time. The advantage of going to a $40\mu s$ as opposed to $10\mu s$ where the uncorrected model is

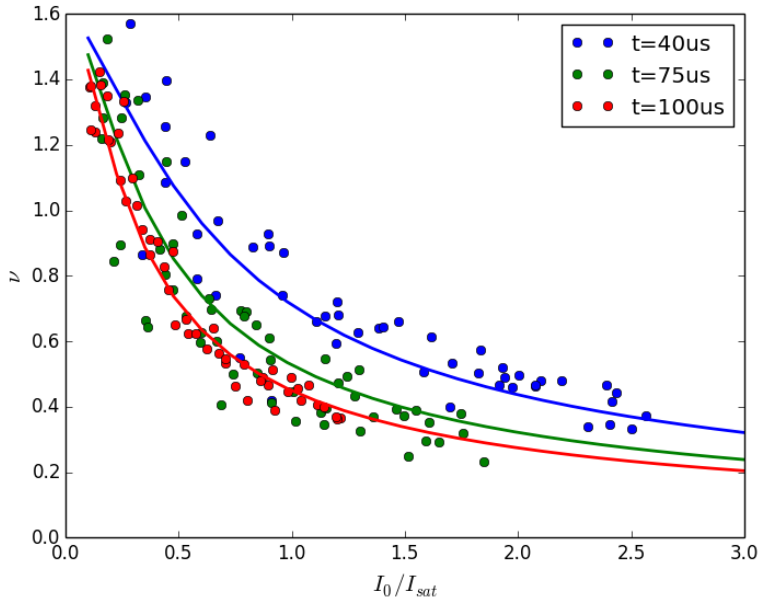

Figure 8. The optical density as a function of probe intensity for three imaging times. The dots represent experimental data and the lines represent the best fit of simulated data. The optimal fit parameters pictured are optical depth of 1.62 and saturation intensity of 29 counts/us.

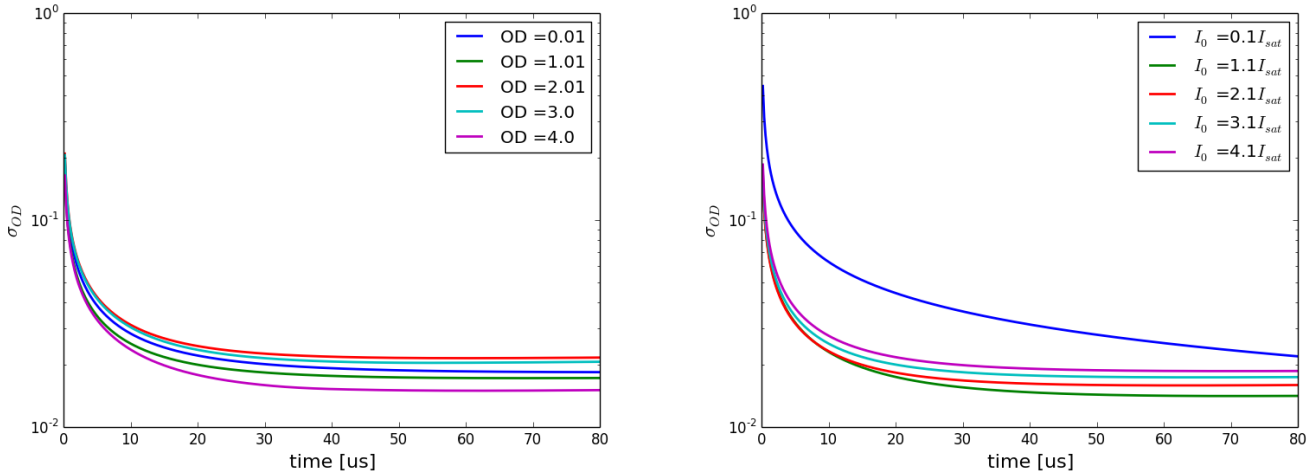

(a) (b)

Figure 9. Dependance of detection uncertainty of optical depth on imaging time, after correcting for recoil induced detuning. a. Uncertainty at fixed probe intensity $I_0/I_{sat} = 2.6$ for a range of optical depths and b. fixed $OD = 1.5$ for a range of probe intensities.

appropriate is about a factor of 1.6 reduction in measurement uncertainty.

3. S-wave scattering experiment

In this section we describe our experiment with scattering two counter-propagating clouds of ^{40}K atoms and observe the resulting s-wave halo of scattered atoms. We vary the magnetic field around the Feshbach resonance during this experiment, and from the change in scattering deduce a location of the magnetic fields resonance of 202.47 Gauss and a width of 8.98 Gauss.

3.1. Experimental procedure

We load our cold Fermi gas of ^{40}K atoms into a crossed dipole trap. We then use adiabatic rapid passage to bring the gas into an equal superposition of $|9/2, -9/2\rangle$ and $|9/2, -7/2\rangle$, the states whose Feshbach resonance we are trying to study.

We then use a large pair of coils in Helmholtz configuration to bring the magnetic field close to the Feshbach resonance, but not close enough for significant collisions to occur. We hold the atoms there to allow the eddy currents in the large coils to settle, and then use a smaller set of Helmholtz coils to hop the field to the desired value. We take two sets of data: one coming from below the resonance, where we hop the large coils to a lower field value than the resonance and use the small coils to hop up to the desired field, and one coming from below the resonance, where we hop the large coils to a field value above the resonance and then use the small coils to hop the field down to the desired value. This allows us to correct for losses due to molecule formation and three-body recombination [1].

We then use a double pulse sequence [8] of a near resonant 1-d retro-reflected optical lattice to transfer most of the atoms into the first two excited states of the lattice, giving them $\pm 2k_r$ of momentum, where k_r is the recoil momentum of the lattice. Since the initial Fermi gas has a wide momentum spread (in contrast to a BEC, which has a very narrow momentum spread), and the lattice pulsing is a momentum dependent process, not all the atoms are successfully transferred into the 1st excited band of the lattice. We optimized our pulse times to minimize the number of atoms that remain in the lowest, zero momentum, band of the lattice, but were not able to eliminate them completely. The optimized pulse times are $23\mu s$ for the first square pulse, $13\mu s$ off interval, and $12\mu s$ for the second square pulse.

We release the atoms from the trap and allow 1ms for the two opposite momentum states within the cloud to pass through each other, scattering on the way. For the data taken coming from below the Feshbach resonance, we then simply ramp down the field and image the atoms. For the data taken coming from above the Feshbach resonance, we then ramp the field back up through the resonance to recover any molecules that were created when the field was ramped from the attractive to the repulsive side of the resonance, and then quickly ramp the field back down and image the atoms. We use an imaging pulse of $40\mu s$.

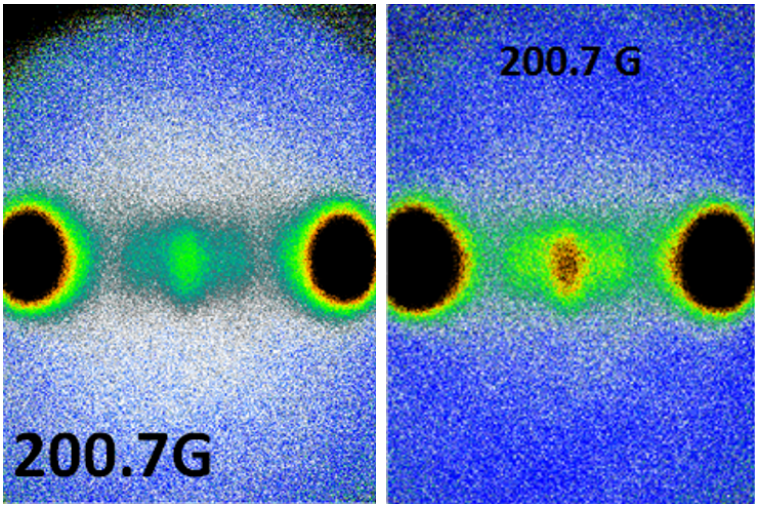

(a) (b)

Figure 10. An example of our absorption image after 6.784ms time of flight. The 1-D lattice is along the horizontal direction at the center of our images. The two large clouds on the left and right are the atoms in the $\pm 2k_r$ momentum orders that passed through each other unscattered. The smaller cloud in the center is the atoms that remained in the lowest band of the lattice after pulsing, and thus obtained no momentum. The thin spread of atoms around these clouds is the atoms that underwent scattering. a. Raw optical density b. Optical density of the same image after correcting for recoil induced detuning by comparing to simulation

3.2. Methods

We first correct each image for recoil induced detuning using the simulation described above. The simulation gives us a look-up table of observed optical density as a function of atom column density and probe intensity. From our two absorption images we observe the probe intensity and optical density for each pixel. We then use the simulation look-up table in an inverted faction to deduce the column density or, equivalently, the optical depth. An example of the effect of this correction procedure in shown in figure 10

To improve the signal and compensate for our shot to shot number fluctuations, we take 15 equivalent images for each data point and, after correcting, add them together. We then perform a standard inverse Abel transform to extract the radial atom number dependence from the two dimensional projection we see in our images. The inverse Abel transform assumes a cilyndrical symmetry, which is present in our case, with the axis of symmetry defined by the 1-D lattice.

We then extract the number of atoms that went through a single scattering event N_{scat}, as a fraction of the total atom number N_{tot}, for each bias magnetic field value. We unscattered number by counting the number of atoms in the two unscattered clouds. We obtain the number of atoms that underwent single scattering by counting the number of atoms outside the Fermi radius of the unscattered clouds, but inside the arc created by rotating the Fermi radius around the original center of the cloud. This method excludes atoms that underwent multiple scatterings, as those atoms are not bound by

momentum concervation to have travelled the same distance from the center as the unscattered clouds in time of flight. The total atom number is the sum of those two.

We then use our data to deduce the resonant field value, the width of the resonance, etc. To do this, we must fit our data to a model. From [1], we have the expression:

$$a(B) = a_{bg}\left(1 - \frac{\Delta}{B - B_0}\right), \tag{11}$$

where a is the scattering length, a_{bg} is the scattering lenth away from the resonance, Δ is the width of the resonance, and B_0 is the field value at which the resonance occurs. Since we are in the low energy regime, the scattering cross-section is given by $\sigma = 4\pi a^2$.

One way to think about the scattering cross-section σ is that the probability P_{scat} that a single particle will get scattered when incident on a cloud of atoms with a surface density of $\frac{N}{A}$ is given by $P_{scat} = \sigma\frac{N}{A}$. If this experiment is repeated 1000 times, the number of times the atom will get scattered is expected to be $N_{scat} = 1000\sigma\frac{N}{A}$. In our case, half the initial cloud, with atoms number $N_{tot}/2$, is incident on the other half of the initial cloud, again with $N_{tot}/2$ atoms. Thus, the number of scattered atoms should be given by $N_{scat} = \frac{N_{tot}}{2}\sigma\frac{N_{tot}}{2} = \sigma\frac{N_{tot}^2}{4A}$, where A is the cross-sectional area of the cloud. Assuming A is constant for all our data, we can absorb the factor of 4A into our definition of a_{bg}, along with the 4π, to obtain

$$\frac{N_{scat}}{N_{tot}^2} = \tilde{a}_{bg}^2\left(1 - \frac{\Delta}{B - B_0}\right)^2. \tag{12}$$

Unfortunately, we cannot fit to this equation directly - camera readout noise is scewed towards the positive, creating an asymetry in detected shot noise for very low and zero atom number pixels. Thus, there is a background number of what looks like scattered atoms in our treatment, giving rise to a background offset o in our data. Thus, the equation we actually fit to is

$$\frac{N_{scat}}{N_{tot}^2} = \tilde{a}_{bg}^2\left(1 - \frac{\Delta}{B - B_0}\right)^2 + o, \tag{13}$$

where our fit parameters are $\tilde{a}_{bg}$, Δ, B_0, and o.

3.3. Results

Our final data is presented in figure 11. The red line is a best fit of the model given in eq.13. The fit parameters we extract are $\tilde{a}_{bg} = 1.48e-3$, $\Delta = 8.98$ Gauss, $B_0 = 202.47$ Gauss, and $o = 9.00e-5$. The error bars on the fitted data are obtained solely from photon shot noise of both absorption images propagated through our analysis. The accepted values for the ^{40}K s-wave Feshbach resonance for the $|9/2, -9/2\rangle$ and $|9/2, -7/2\rangle$ states are $B_0 = 202.1 \pm 0.07$ and $\Delta = 7.8 \pm 0.6$.

4. Conclusion

We studied the effects of recoil-induced detuning effects on absorption images and found an optimal imaging time of $40\mu s$ for ^{40}K atoms for noise minimization after corrections.

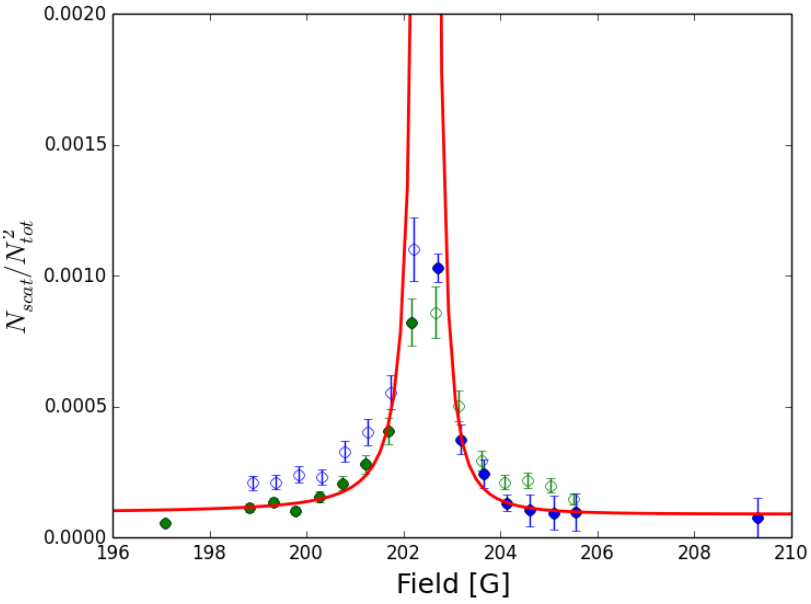

Figure 11. Scattered fraction over the total atom number as a function of bias field. Green dots represent data taken coming from below the resonance, and blue dots represent the data taken coming from above the resonance. Red is the line of best fit, where data coming from above the resonance was used above the resonance and data coming from below the resonance was used below the resonance to create the fit. The four points in the middle were not used in the fit at all, as they are in the regime where the scattering length is large enough for the atoms to behave hydrodynamically and the assumption $\sigma\rho \ll 1$, where ρ is the atom number per unit area, is no longer valid.

We use these results to observe s-wave scattering halos of the Fermi gas around the Feshbach resonance and directly verify the resonance location and width. Our analysis can be used in any absorption imaging applications where signal to noise minimization is critical. Experimental techniques devoloped for our s-wave scattering expeiment can be readily extended to a Raman-coupled single component gas version, in which we hope to detect synthetic p-wave interactions.

Acknowledgements

We thank Marcell Gall for helpful discussions. This work was supported by ???

References

[1] Cheng Chin, Rudolf Grimm, Paul Julienne, and Eite Tiesinga. Feshbach resonances in ultracold gases. *Rev. Mod. Phys.*, 82:1225–1286, Apr 2010.

[2] Lindsey J. LeBlanc. *Exploring many-body physics with ultracold atoms.* PhD thesis, University of Toronto, 2011.

[3] C. Monroe, E. Cornell, C. Sackett, C. Myatt, and C. Wieman. Measurement of cs-cs elastic scattering at T =30 μk. *Phys. Rev. Lett.*, 70:414–417, Jan 1993.

[4] K. M. O'Hara, S. L. Hemmer, M. E. Gehm, S. R. Granade, and J. E. Thomas. Observation of a strongly interacting degenerate fermi gas of atoms. *Science*, 298(5601):2179–2182, 2002.

[5] C. Regal and D. Jin. Measurement of positive and negative scattering lengths in a fermi gas of atoms. *Phys. Rev. Lett.*, 90:230404, Jun 2003.

[6] G. Reinaudi, T. Lahaye, Z. Wang, and D. Guéry-Odelin. Strong saturation absorption imaging of dense clouds of ultracold atoms. *Opt. Lett.*, 32(21):3143–3145, Nov 2007.

[7] R. A. Williams, L. J. LeBlanc, K. Jimnez-Garca, M. C. Beeler, A. R. Perry, W. D. Phillips, and I. B. Spielman. Synthetic partial waves in ultracold atomic collisions. *Science*, 335(6066):314–317, 2012.

[8] Saijun Wu, Ying-Ju Wang, Quentin Diot, and Mara Prentiss. Splitting matter waves using an optimized standing-wave light-pulse sequence. *Phys. Rev. A*, 71:043602, Apr 2005.